AFRL-AFOSR-VA-TR-2022-0453

Nonreciprocal Structures with Phase-Change Components

Chabanov, Andrey
University of Texas at San Antonio
One Utsa Circle
San Antonio, TX, 78249-1130
US

08/02/2022
Final Technical Report

Air Force Research Laboratory
Air Force Office of Scientific Research
Arlington, Virginia 22203
Air Force Materiel Command

REPORT DOCUMENTATION PAGE

PLEASE DO NOT RETURN YOUR FORM TO THE ABOVE ORGANIZATION.

1. REPORT DATE	2. REPORT TYPE	3. DATES COVERED	
20220802	Final	START DATE 20190815	END DATE 20220214

4. TITLE AND SUBTITLE
Nonreciprocal Structures with Phase-Change Components

5a. CONTRACT NUMBER	5b. GRANT NUMBER	5c. PROGRAM ELEMENT NUMBER
	FA9550-19-1-0359	61102F
5d. PROJECT NUMBER	**5e. TASK NUMBER**	**5f. WORK UNIT NUMBER**

6. AUTHOR(S)
Andrey Chabanov

7. PERFORMING ORGANIZATION NAME(S) AND ADDRESS(ES)
University of Texas at San Antonio
One Utsa Circle
San Antonio, TX 78249-1130
US

8. PERFORMING ORGANIZATION REPORT NUMBER

9. SPONSORING/MONITORING AGENCY NAME(S) AND ADDRESS(ES)	10. SPONSOR/MONITOR'S ACRONYM(S)	11. SPONSOR/MONITOR'S REPORT NUMBER(S)
Air Force Office of Scientific Research 875 N. Randolph St. Room 3112 Arlington, VA 22203	AFRL/AFOSR RTB1	AFRL-AFOSR-VA-TR-2022-0453

12. DISTRIBUTION/AVAILABILITY STATEMENT
A Distribution Unlimited: PB Public Release

13. SUPPLEMENTARY NOTES

14. ABSTRACT
This project included two thrust areas: Reflective mm-wave photonic limiter and Magnetooptical composite materials with zero net magnetization. Jointly with the Directed Energy and Sensors Directorates of AFRL, we have demonstrated a free-space, reflective mmwave limiter based on a multilayer structure involving a nanolayer of a phase-change material, vanadium dioxide, which experiences a heat-related insulator-to-metal transition. The multilayer acts as a variable reflector, controlled by the incident wave intensity. At low intensities, VO2 remains dielectric, and the multilayer exhibits strong resonant transmittance. When the incident intensity exceeds a threshold level, the emerging metallic phase renders the multilayer highly reflective while safely dissipating a small portion of the input power without damage to the limiter. In addition, we have identified a way of cutting down the limiter's activation time by more than three orders of magnitude, which is critically important for military applications. Pending further study, the proposed approach can lead to the experimental demonstration of ultrafast broadband limiters to protect sensitive electronics from high-power microwave radiation. We have designed and conducted proof-of-concept measurements of magnetic composite material with strong nonreciprocal characteristics, such as Faraday rotation, while having zero magnetization and not requiring a bias magnetic field. Our approach (U.S. patent pending) is based on a composite structure made of two different magnetic materials: magnetically hard and strongly anisotropic material (e.g., Nd) and magnetically soft material displaying low losses at operational frequencies (e.g., YIG at microwave frequencies). The idea is that only one (magnetically soft) of the two constitutive materials efficiently interacts with the electromagnetic oscillations and, thereby, contributes to the nonreciprocal properties, such as Faraday rotation. The role of the other (magnetically hard) constitutive component is to provide the magnetic bias for the first component and to offset the net magnetization of the composite structure. This groundbreaking work shall aid in designing a magnetization-free Faraday rotator at both microwave frequencies and optical wavelengths.

15. SUBJECT TERMS

16. SECURITY CLASSIFICATION OF:			17. LIMITATION OF ABSTRACT	18. NUMBER OF PAGES
a. REPORT	b. ABSTRACT	c. THIS PAGE		
U	U	U	UU	10

19a. NAME OF RESPONSIBLE PERSON	19b. PHONE NUMBER *(Include area code)*
ALI SAYIR	426-7236

Report Coversheet
FA9550-19-1-0359

Reporting Periods
Start 15 Aug 2019- End 14 May 2022

Distribution Statement
Distribution A - Approved For Public Release

Program Officer Name
Dr. Ali Sayir

Principal Investigator Name
Dr. Andrey Chabanov

Project Title
Nonreciprocal Structures with Phase-Change Components

ABSTRACT

This project included two thrust areas: *Reflective mm-wave photonic limiter* and *Magnetooptical composite materials with zero net magnetization*.

Jointly with the Directed Energy and Sensors Directorates of AFRL, we have demonstrated a free-space, reflective mm-wave limiter based on a multilayer structure involving a nanolayer of a phase-change material, vanadium dioxide, which experiences a heat-related insulator-to-metal transition. The multilayer acts as a variable reflector, controlled by the incident wave intensity. At low intensities, VO_2 remains dielectric, and the multilayer exhibits strong resonant transmittance. When the incident intensity exceeds a threshold level, the emerging metallic phase renders the multilayer highly reflective while safely dissipating a small portion of the input power without damage to the limiter. In addition, we have identified a way of cutting down the limiter's activation time by more than three orders of magnitude, which is critically important for military applications. Pending further study, the proposed approach can lead to the experimental demonstration of ultrafast broadband limiters to protect sensitive electronics from high-power microwave radiation.

We have designed and conducted proof-of-concept measurements of magnetic composite material with strong nonreciprocal characteristics, such as Faraday rotation, while having zero magnetization and not requiring a bias magnetic field. Our approach (U.S. patent pending) is based on a composite structure made of two different magnetic materials: magnetically hard and strongly anisotropic material (e.g., Nd) and magnetically soft material displaying low losses at operational frequencies (e.g., YIG at microwave frequencies). The idea is that only one (magnetically soft) of the two constitutive materials efficiently interacts with the electromagnetic oscillations and, thereby, contributes to the nonreciprocal properties, such as Faraday rotation. The role of the other (magnetically hard) constitutive component is to provide the magnetic bias for the first component and to offset the net magnetization of the composite structure. This groundbreaking work shall aid in designing a magnetization-free Faraday rotator at both microwave frequencies and optical wavelengths.

Final Report

Reflective mm-wave photonic limiter.

Millimeter wave (mm-wave) communications and radar receivers capable of processing small signals must be protected from high-power signals, damaging sensitive receiver components. Many of these systems arguably can be protected by using photonic limiting techniques.

Optical limiting is a technique to protect photosensitive devices from damage caused by intense optical radiation [1,2]. Optical limiters are therefore designed to block high-intensity laser radiation while transmitting low-intensity light. Most passive optical limiters utilize materials with nonlinear absorption, which are transparent to low-intensity light but turn opaque if the light intensity exceeds a certain (limiting) threshold level [3-5]. A typical passive limiter, however, absorbs a significant portion of high-level radiation, which can cause overheating and damage to the limiter itself [2,6].

To overcome this problem, the concept of a reflective photonic limiter, which reflects rather than absorbs high-intensity radiation, has been introduced [7-9]. A passive reflective photonic limiter involves a photonic bandgap structure, such as a multilayer cavity, incorporating a nonlinear [9,10] or a phase-change material (PCM) [11,12]. At low intensities, the photonic structure displays a strong resonant transmittance. High-intensity radiation, however, forces nonlinearity to kick in or phase transition to be induced, producing an impedance mismatch resulting in a strong broadband reflectivity. The high reflectivity prevents the limiter from overheating, thereby significantly increasing the limiter damage threshold. Other significant advantages of the photonic design include orders-of-magnitude larger extinction ratio (the ratio of transmittances below and above the limiting threshold), and the possibility to significantly lower the limiting threshold by adjusting the photonic structure hosting the nonlinear material or a PCM. The approach mentioned above thus provides advanced broadband protection from high-level radiation, although low-intensity transmission is essentially narrowband due to its resonant nature. Arguably, free-space mm-wave limiters can be designed in much the same way to protect systems receivers from high-power signals and also to allow the receivers to function normally when these high-power signals are not present.

In Ref. [13], we have designed and demonstrated a free-space, reflective photonic limiter for the W band. The proposed photonic limiter is a resonant air/sapphire multilayer structure, incorporating a 150-nm VO_2 layer undergoing an insulator-to-metal transition when heated above the critical temperature, $\theta_c \approx 69℃$ [Fig. 2 (A and B)]. The multilayer structure is so thin (a few mm) that it can be used to cover a wide area, such as a phase antenna array. The limiter acts as a variable reflector, controlled by the incident wave intensity I_0. If I_0 is below a certain threshold level I_t, the VO_2 layer remains in the dielectric state, and the multilayer exhibits high transmittance in a finite frequency band, even though a small portion of I_0 is absorbed by the multilayer, leading to the initial heating of VO_2 [Fig. 2 (C and E)]. When I_0 exceeds I_t, a fraction of the VO_2 layer transitions into the metallic phase with sharply increased electrical conductivity, rendering the entire multilayer highly reflective [Fig. 2 (D and F)].

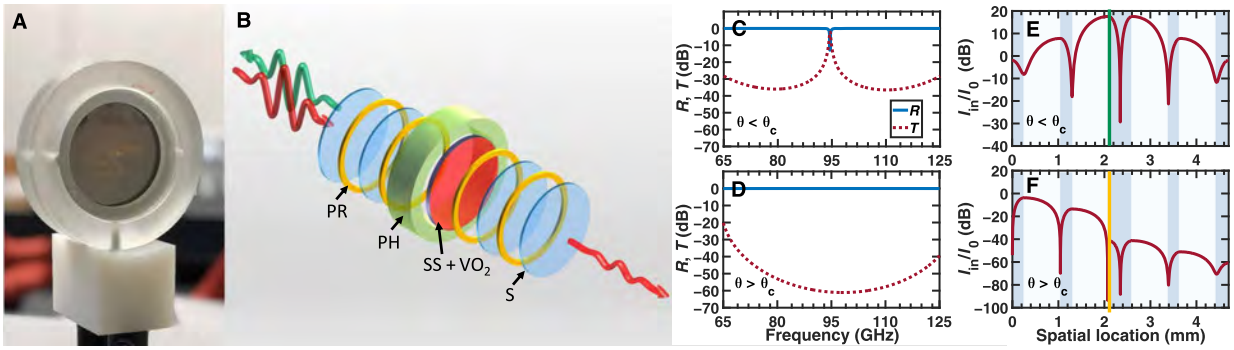

Fig. 2. Reflective mm-wave photonic limiter. A picture (**A**) and schematic (**B**) of the mm-wave photonic limiter consisting of 256-μm-thick (S) and 525-μm-thick (SS) sapphire wafers separated by 792-μm air-gap spacers (PR) and a 150-nm VO_2 layer deposited on the SS sapphire. The layer stack is retained in a plastic holder (PH). (**C** and **D**) Simulated transmittance T and reflectance R of the photonic structure at normal incidence, at $\theta > \theta_C$ (C) and $\theta < \theta_C$ (D). (**E** and **F**) Simulated internal intensity profiles in the direction of wave propagation of the incident intensity I_0 at the resonance frequency 95 GHz, at $\theta > \theta_C$ (E) and $\theta < \theta_C$ (F). Sapphire and air-gap layers are shown in dark and light blue, and the VO_2 layer in green and yellow at the lower and higher temperatures, respectively.

The reflective mm-wave limiter has been tested by a high-power CW source at 95 GHz. Figure 3A shows linear-log plots of the transmitted power $P_T(t)$ for incident Gaussian beams of a waist radius of 16.5 mm and input powers $P_0 = 30$, 35, 40, 45, and 55 W. For each input power, $P_T(t)$ is seen to initially increase and then decrease with time. This is due to the fact that the transmission resonance shifts to lower frequencies with increasing temperature. In addition, at input powers $P_0 > 30$ W, $P_T(t)$ exhibits a sharp drop associated with the insulator-to-metal transition in the VO_2 layer. The corresponding transition or switching time, t_s, is plotted versus P_0 in the inset; notice that at 30 W input power, the transition is not manifested in $P_T(t)$. The shortest switching time observed in these proof-of-concept measurements was about 7 s at the highest available input power of 55 W.

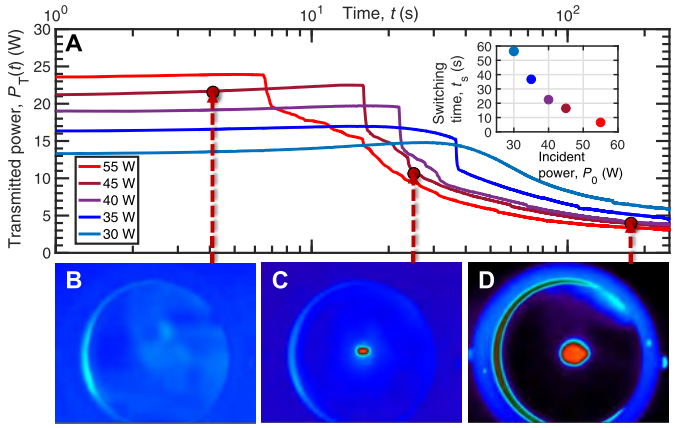

Fig. 3. High-power mm-wave measurements of the photonic limiter. (**A**) Time-varying transmitted power $P_T(t)$ of the photonic limiter following excitation by a CW 95-GHz Gaussian beam with the waist radius r_0= 16.5 mm and input powers P_0 = 30, 35, 40, 45, and 55 W. Inset: Switching time t_S, corresponding to the onset of the metallic phase in the VO_2 layer, versus the input power P_0. (**B** to **D**) Thermal images of the limiter front end at the elapsed times indicated by the respective dashed arrows in (A), for P_0 = 45 W.

The transition in the VO_2 layer was observed with a FLIR thermal camera which could distinguish between the dielectric and metallic phases of VO_2 because of their different emissivities in the infrared. Figure 3 (B to D) displays thermal images of the limiter front end at elapsed times

indicated by dashed arrows in Fig. 3A for the incident power of 45 W. The first occurrence of the metallic phase in the center of the VO_2 layer (red spot in Fig. 3A) coincides with the sharp drop in $P_T(t)$. Then the metallic domain grows in size (Fig. 3D), accompanied by a further decrease in $P_T(t)$, until thermal equilibrium is reached. When high input power is no longer present, the VO_2 reverts from the metallic to the dielectric phase after a brief delay.

The experimental data of Fig. 3 are in good agreement with 3D multiphysics simulations. Figure 4 shows the computed time-dependent transmitted power $P_T(t)$, reflected power $P_R(t)$, and absorptance $A(t) = (P_0 - P_T(t) - P_R(t))/P_0$ of the limiter following excitation by a 95-GHz Gaussian beam of input powers $P_0 = 29$, 56, 554, and 5540 W. $P_T(t)$ exhibits abrupt, steep decrease once VO_2 has reached θ_c (Fig. 4A). Also, in the steady limiting regime (flat portion of the curves at later times) the input power is reflected to a greater extent than is absorbed [Fig. 5 (B and C)]. We further note in Fig. 4A that the switching time is inversely proportional to the input power, $t_s \propto 1/P_0$, and that at $t > t_s$, the transmitted power decreases inversely with time, $P_T(t) \propto 1/t$ (shown by a dotted black line). The dependence of t_s on P_0 can be understood from the solution of a heat balance equation for the VO_2 layer in the beam center [13].

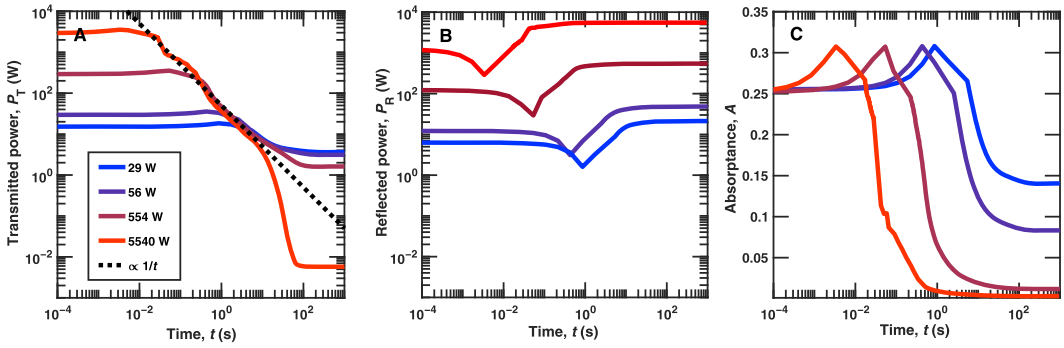

Fig. 4. Simulated temporal response of the photonic limiter under monochromatic excitation. (**A** to **C**) Time evolution of the transmitted power $P_T(t)$ (A), reflected power $P_R(t)$ (B), and absorptance $A(t)$ (C) of the limiter following excitation by a 95-GHz Gaussian beam with the waist radius r_0 = 16.5 mm and input powers P_0 = 29, 56, 554, and 5540 W. The black dashed line in (A) indicates a slope of $P_T(t) \propto 1/t$.

As seen from Fig. 4C, the resonant setting of the multilayer enhances the initial (low-temperature) absorptance by two orders of magnitude compared to the stand-alone VO_2-on-sapphire wafer. In the presence of continuous input power P_0, $A(t)$ rises up to a peak of ~0.32 regardless of P_0 and then falls down to a constant level depending on P_0. This absorptance behavior, which is characteristic of the entire multilayer rather than the stand-alone VO_2-on-sapphire wafer, is essential to understanding the mm-wave limiting process in the photonic limiter. The increase in absorptance resulting from the heating effect triggers thermal runaway, in which the VO_2 temperature quickly runs up to θ_c and higher, carrying VO_2 through the phase transition. When I_0 exceeds I_t, a fraction of the VO_2 layer transitions into the metallic phase with sharply increased electrical conductivity, rendering the entire multilayer highly reflective. The time t_s before the transition starts is inversely proportional to the incident intensity, $t_s \propto 1/I_0$, after which the multilayer is brought to equilibrium by a combination of positive and negative feedbacks between mm-wave absorption and heating of VO_2. For a given intensity $I_0 \geq I_t$, the equilibrium is determined by the fraction of the VO_2 layer transformed into the metallic phase. At that point, the limiter is capable of safely dissipating a small portion of the incident power absorbed by the limiter while reflecting the rest of the energy back to space. The high reflectivity (as opposed to

absorptance) prevents the limiter from overheating. Moreover, a combination of the resonant conditions and the high contrast in electrical conductivity between the two phases of VO_2 results in a significant enhancement of the limiter extinction ratio and allows a drastic reduction in the limiting threshold – both highly desirable features in limiting applications.

The limiter properties, such as operating frequency, bandwidth, threshold level, and switching time, are determined by the limiter design, ambient conditions, and incident power density. In particular, as long as the VO_2 nanolayer is in the dielectric phase, most of the resonant absorption occurs in the sapphire substrate, while the VO_2 contributions to the absorption and heating processes remain negligible. The relatively large thickness of the sapphire substrate (~0.5 mm) results in its large heat capacity, which explains the long switching times of the limiter. If the damage inflicted by HPM is thermal in origin, a critically important characteristic of the free-space limiter is the energy density passed through the limiter before the limiter blocks the input radiation, $U = I_0 t_s$, where $t_s \propto 1/I_0$. It thus turns out that if the incident intensity I_0 is well above the limiting threshold, the value of U is virtually independent of I_0, $U \approx C(\theta_c - \theta_0)/A$, provided that t_s is much shorter than the temperature relaxation time of the limiter. Given the specific parameters of our limiter and the ambient temperature, the total transmitted energy density U during the limiter switching time t_s is ~ 22.5 J/cm^2. One way to substantially reduce both the switching time t_s and the passed energy density U would be to deposit a resistive nanolayer or nanostructure [14] on the top of the VO_2. The heat capacity of the resistive nanolayer can be much smaller than that of the sapphire substrate (e.g., by four orders of magnitude in the case of In_2O_5Sn), and the heat released in the resistive nanolayer will be almost instantly transferred to the VO_2 nanolayer. Preliminary estimates show the reduction in t_s and U of more than three orders of magnitude, particularly for the incident intensity I_0 well above the limiting threshold (it can still be well below the damage threshold). Pending further study, this preliminary estimate may lead to ultrafast, broadband reflective limiters with enhanced dynamic range.

Magnetooptical composite materials with tunable and zero net magnetization.

The critical component of most nonreciprocal devices, such as microwave and optical isolators, circulators, and nonreciprocal phase shifters, is a magneto-optical material placed in an external magnetic field [15-17]. This traditional approach involves using bulky magnets, which can be a significant problem, especially in small devices. Alternatively, one can use permanently magnetized materials, such as ferrites or ferromagnets with high coercivity. Such materials display nonreciprocal electromagnetic properties even without an external bias magnetic field. The magnetized material, however, creates its own demagnetization field, which depends on its shape and can be nonuniform unless the shape of the magnetized component is strictly ellipsoidal. The field non-uniformity inside magneto-optical material can seriously compromise the performance of the isolator or any other nonreciprocal device. Another common problem with both externally biased and self-biased approaches is related to the existence of a relatively strong magnetic field inside and outside the magneto-optical component. There are some important applications/ devices, such as quantum navigation and sensing [18], which cannot tolerate even a tiny magnetic field, but they still require nonreciprocal components for optical isolation or other nonreciprocal functionalities. This project addresses the above problems by introducing a composite material with strong nonreciprocal characteristics, such as Faraday rotation, while having zero magnetization and not requiring a bias magnetic field. In this respect, our approach is qualitatively new (U.S. patent pending [19]). That said, this technology is still in its infancy, and many unresolved questions need to be addressed.

There exists a natural solution to the above problems — the so-called compensated ferrites, which have zero net magnetization while producing a significant magnetic Faraday rotation even in the absence of a bias magnetic field. Such single-phased materials usually comprise two magnetic subsystems (magnetic sublattices) involving different kinds of magnetic ions. The first magnetic subsystem comprises magnetic ions of the iron group (3d-ions). At room temperatures, the respective magnetic sublattices are saturated and have nonzero combined magnetization. The second magnetic subsystem includes rare-earth ions (4f-ions) with the combined magnetization equal and opposite to that of the first magnetic subsystem. Despite zero net magnetization, such compensated ferrites can produce sufficiently strong magnetic Faraday rotation and, hence, can be used in nonreciprocal applications. Examples of the kind are provided by some rare-earth orthoferrites [20] and garnets [21] (for instance, Ce-doped garnet $Tb_3Fe_5O_{12}$). There are, however, several fundamental problems with such single-phased compensated magneto-optical materials.

The first inherent problem stems from the fact that while the first iron magnetic subsystem is fully saturated at room temperatures, the second rare-earth magnetic subsystem is far from saturation. For this reason, while the combined magnetization of the first magnetic subsystem is fixed, the contribution of the rare-earth magnetic subsystem to the net magnetization is temperature-dependent. As a consequence, the state with zero net magnetization can only be realized at a magnetic compensation temperature, T_{comp}. At $T > T_{comp}$ and $T < T_{comp}$, the net magnetization of the ferrite reappears. Besides, due to the reappearing net magnetization, the ferrite might develop domain structure, which can sharply increase absorption while reducing or even completely eliminating the Faraday rotation. The second problem with all rare-earth ferrites is that not only their magnetization but also their contribution to Faraday rotation is highly dependent on temperature.

To address the above problems, we put forward a qualitatively different approach to achieving a strong Faraday rotation without a bias field in a material with zero net magnetization. Our approach is based on composite structures made up of two different magnetic materials. In the case of microwave applications, the constitutive materials must satisfy the following two conditions:

1. One of the constitutive materials is magnetically hard and strongly anisotropic (for example, Nd), while the other one is magnetically soft and displays low losses at operational frequencies (for example, YIG at microwave frequencies).
2. The Curie temperatures of both magnetic materials must be high enough for them to be magnetically saturated at room temperature. This condition ensures that zero net magnetization of the composite is maintained within a broad temperature range, while the Faraday rotation per unite length also remains temperature independent.

The idea is that only one of the two constitutive materials (the magnetically soft one) efficiently interacts with the electromagnetic oscillations and, thereby, contributes to the nonreciprocal properties, such as Faraday rotation. The role of the other (magnetically hard) constitutive component is two-fold: (a) it provides the magnetic bias for the first component, and (b) it offsets the net magnetization of the composite structure.

The proposed material realization that simultaneously biases a ferrite and generates a non-reciprocal response such as Faraday rotation (i.e., linearly polarized radiation rotates as it propagates through the ferrite) is shown in Fig. 5. The dark blue cylinders represent metal-plated neodymium (Nd) permanent magnets that bias the green YIG slab with a z-directed magnetic field; the violet Rexolite serve as impedance matching layers. From a macroscopic point of view, the ferrite appears to be self-biased because we have removed the bulky external magnets and

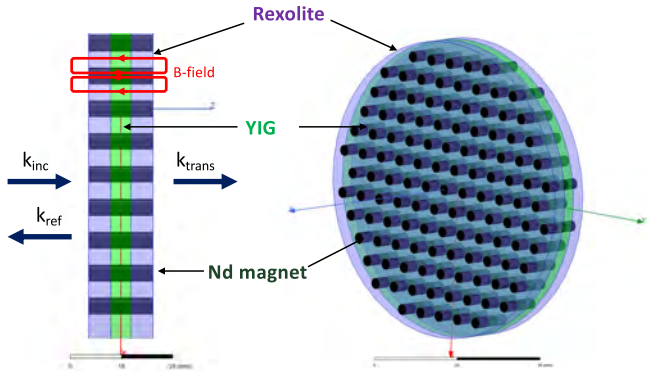

Fig. 5. Magnetization-free Faraday rotator. The dark blue cylinders represent metal-plated neodymium (Nd) permanent magnets that bias the green YIG slab with a z-directed magnetic field. The violet Rexolite serve as impedance matching layers. The magnetic compensation filling fraction f_{comp} of Nd magnets ensures that the Faraday rotator has zero net magnetization.

integrated them directly into the ferrite. We can tune the YIG's magnetic properties by engineering the magneto-static bias field strength. This bias field is controlled by choice of permanent magnet material and the filling fraction of the permanent magnet area to the unit cell area. At the magnetic compensation filling fraction f_{comp}, the material configuration of Fig. 5 has zero net magnetization.

The Faraday rotator of Fig. 5 has been realized (Fig. 6) and tested by the measurement system. In fabricating the composite structure, we faced a limitation of the available minimum size (0.125" diameter) of Nd magnets, leading to a trade-off between the Nd system magnetization and the distance between the neighboring Nd cylinders. In particular, we have achieved a net magnetization of 0.9 kG, rather than zero net magnetization, because $f > f_{comp}$. Reducing f by increasing the distance between the neighboring Nd rods would lead to structural effects on transmission at 11 GHz, where Faraday rotation is 45°.

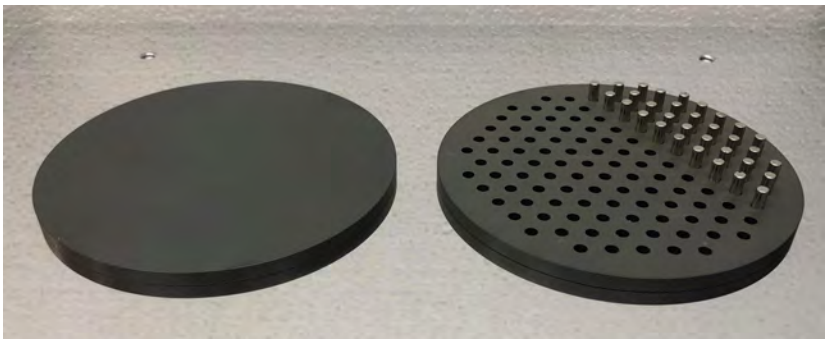

Fig. 6. Composite Faraday rotator. 4" YIG disks of thickness 0.165", solid (left) and with 0.125" diam. holes filled with Nd magnets. Whereas the solid disk requires external magneto-static bias, the composite material appears self-biased by Nd magnets integrated directly into the ferrite.

The experimental setup and microwave transmission measurement of the YIG solid disk in a magnetic field of 0.9 kG and the composite YIG/Nd disk in the absence of a magnetic field are shown in Fig. 7 A and B, respectively. Indeed, there is good agreement between the two measurements, indicating that bulky external magnets can be removed and integrated directly into

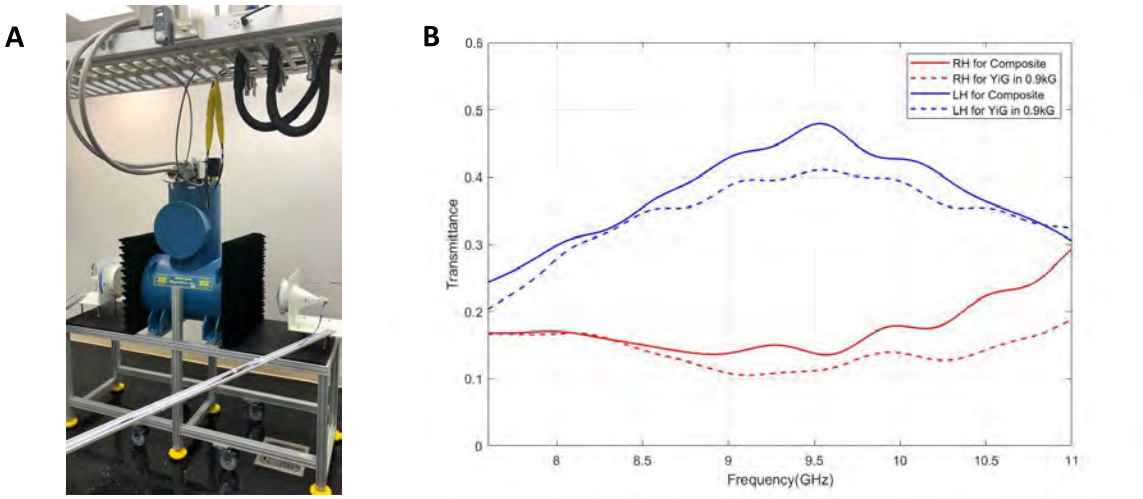

Fig. 7. (**A**) Experimental setup and (**B**) microwave transmission measurements via the YIG solid disk in magnetic field 0.9 kG (solid) and composite YIG/Nd disk in absence of magnetic field (dashed) for right- (red) and left-handed (blue) polarizations.

ferrite. Moreover, by changing the Nd filling fraction f, one can control the spectral range of the Faraday rotator.

Figure 8 shows the isolation/circulation functionality of the composite YIG/Nd disk in the X band. In the measurement performed without any magnetic field, the disk was placed between two linearly polarized horn antennas making a 45° angle with each other and thus acting as two polarizers. A linearly polarized wave propagating in the forward direction (i.e., parallel to the net magnetization) shows low insertion loss, as measured by the receiving antenna. In contrast, the wave propagating in the opposite direction exhibits a more than 25 dB isolation at 11 GHz. The measurements are in good agreement with simulation results shown by dashed lines.

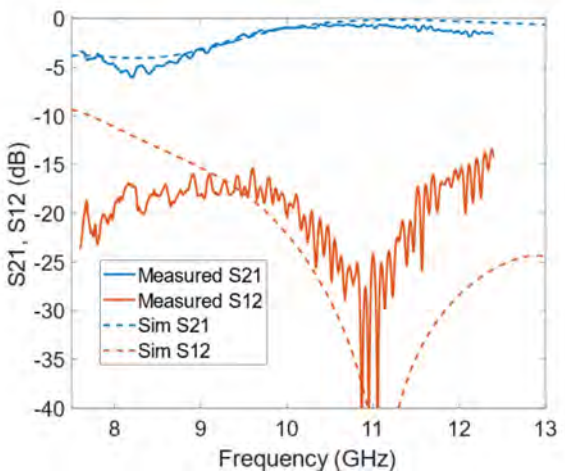

Fig. 8. Isolation/circulation functionality of the composite YIG/Nd disk in the X band. Scattering coefficients S_{21} (blue) and S_{12} (red) of the YIG/Nd disk in the absence of magnetic field, indicating low insertion loss in forward direction and more than 25 dB isolation in the backward direction. The dashed lines are simulation results.

The results of Fig. 8 represent a qualitatively new approach to magneto-optical materials and devices. In particular, we have been evaluating a transmitter/receiver (Tx/Rx) which combines an orthomode transducer, low gain dual-polarized feed antenna, a dielectric lens, and the impedance matched magnetization-free Faraday rotator. In our proposed geometry, the Tx/Rx isolation is predominately determined by the isolation of the orthomode transducer, which is often > 40 dB. In contrast, the Tx/Rx isolation of the conventional system is limited by the impedance match of the horn antenna and is usually < 20 dB. Therefore, we expect a 20 dB isolation improvement using our proposed system compared to the reference system. In parallel, we have been working on a more uniform composite material design involving porous materials (like aluminum oxide and polycarbonate matrix) incorporating magnetic metal (Co, Ni) nanorods. This 'metamaterial' approach is expected to eliminate any structural effects on wave transmission.

References:

[1] L. W. Tutt, T. F. Boggess, A review of optical limiting mechanisms and devices using organics, fullerenes, semiconductors and other materials. *Prog. Quantum. Electron.* **17**, 299-338 (1993).

[2] M. J. Miller, A. G. Mott, B. P. Ketchel, General optical limiting requirements. *Proc. SPIE* **3472**, 24-29 (1998).

[3] E. W. Van Stryland, Y. Y. Wu, D. J. Hagan, M. J. Soileau, K. Mansour, Optical limiting with semiconductors. *J. Opt. Soc. Am. B* **5**, 1980-1988 (1988).

[4] L. W. Tutt, A. Kost, Optical limiting performance of C_{60} and C_{70} solutions. *Nature* **356**, 225-226 (1992).

[5] P. Chen, X. Wu, X. Sun, J. Lin, W. Ji, K. L. Tan, Electronic structure and optical limiting behavior of carbon nanotubes. *Phys. Rev. Lett.* **82**, 2548 (1999).

[6] T. Boggess, A. Smirl, S. Moss, I. Boyd, E. Van Stryland, Optical limiting in GaAs. *IEEE J. Quantum Electron.* **21**, 488-494 (1985).

[7] E. Makri, H. Ramezani, T. Kottos, I. Vitebskiy, Concept of a reflective power limiter based on nonlinear localized modes. *Phys. Rev. A* **89**, 031802 (2014).

[8] E. Makri, T. Kottos, I. Vitebskiy, Reflective optical limiter based on resonant transmission. *Phys. Rev. A* **91**, 043838 (2015).

[9] J. H. Vella, J. H. Goldsmith, A. T. Browning, N. I. Limberopoulos, I. Vitebskiy, E. Makri, T. Kottos, Experimental realization of a reflective optical limiter. *Phys. Rev. Applied* **5**, 064010 (2016).

[10] S. Suwunnarat, R. Kononchuk, A. Chabanov, I. Vitebskiy, N. I. Limberopoulos, T. Kottos, Enhanced nonlinear instabilities in photonic circuits with exceptional point degeneracies. *Photonics Res.* **8**, 737-744 (2020).

[11] R. Thomas, A. A. Chabanov, I. Vitebskiy, T. Kottos, Light-induced optical switching in an asymmetric metal-dielectric microcavity with phase-change material. *EPL* **126**, 64003 (2019).

[12] N. Antonellis, R. Thomas, M. A. Kats, I. Vitebskiy, T. Kottos, Nonreciprocity in photonic structures with phase-change components. *Phys. Rev. Applied* **11**, 024046 (2019).

[13] R. Kononchuk, S. Suwunnarat, M.S. Hilario, A.E. Baros, B.W. Hoff, V. Vasilyev, I. Vitebskiy, T. Kottos, A.A. Chabanov, A reflective mm-wave photonic limiter, *Sci. Adv*. **8**, abh1827 (2022).

[14] L. Kong, Z. Li, L. Liu, R. Huang, M. Abshinova, Z. Yang, C. B. Tang, P. Tan, C. Deng, S. Matitsine, Recent progress in some composite materials and structures for specific electromagnetic applications. *Int. Mater. Rev.* **58**, 203-259 (2013).

[15] K. Chang, *Handbook of microwave and optical components* (Wiley, 1989).

[16] D. A. Pozar, *Microwave Engineering* (John Wiley, 1998).

[17] A. K. Zvezdin and V. A. Kotov, *Magnetooptics and Magnetooptical Materials* (Taylor & Francis, 1997).

[18] A. Cameron, Quantum magnetometer senses its place, *GPS World*, May 18, 2019 [https://www.gpsworld.com/quantum-magnetometer-senses-its-place/]

[19] A. A. Chabanov, C. Pfeiffer, I. Anisimov, and I. Vitebskiy, Magnetization free Faraday rotator, US 63/262,896 (pending).

[20] H. J. Zhao, J. Íñiguez, X. M. Chen, and L. Bellaiche, Origin of the magnetization and compensation temperature in rare-earth orthoferrites and orthochromates, *Phys. Rev. B* **93**, 014417 (2016).

[21] R. W. Cooper, W. A. Crossley, J. L. Page, and R. F. Pearson, "Faraday Rotation in YIG and TbIG", *J. Appl. Phys.* **39**, 565 (1968).